DEC 05 1997

MASTER COPY KEEP THIS COPY F

AFRL-SR-BL-TR-98-

0076

DEC 05 1997

REPORT DOCUMENTATION PA

Public reporting burden for this collection of information is estimated to average 1 hour per res... gathering and maintaining the data needed, and completing and reviewing the collection of inf... collection of information, including suggestions for reducing this burden, to Washington Heade... Davis Highway, Suite 1204, Arlington, VA 22202-4302, and to the Office of Management and Bu...

...4-0188

...isting data sources, ...other aspect of this ...orts, 1215 Jefferson ...Washington, DC 20503

1. AGENCY USE ONLY (Leave blank)	2. REPORT DATE	3. REPORT TYPE AND DATES COVERED
	Dec 1, 1998	Final Report, June 1, 1996-Aug. 31, 1997

4. TITLE AND SUBTITLE

Pressure Sensor Arrays and Microactuators for Fluid Mechanics Research

5. FUNDING NUMBERS

F49620-96-0293

6. AUTHOR(S)

Khalil Najafi, C. Huang

7. PERFORMING ORGANIZATION NAME(S) AND ADDRESS(ES)

The Regents of the University of Michigan
Ann Arbor MI 48109

8. PERFORMING ORGANIZATION REPORT NUMBER

9. SPONSORING/MONITORING AGENCY NAME(S) AND ADDRESS(ES)

Air Force Office of Scientific Research
(AFOSR) Bolling AB
Washington DC 20332-6448

NA

10. SPONSORING/MONITORING AGENCY REPORT NUMBER

11. SUPPLEMENTARY NOTES The views and conclusions contained herein are those of the authors and should not be interpreted as necessarily representing the official policiies or endorsements, either expressed or implied, of the Air Force Office of Scientific Research or the US Government.

12a. DISTRIBUTION/AVAILABILITY STATEMENT

Distribution Statement A. Approved for public release; distribution is unlimited.

12b. DISTRIBUTION CODE

13. ABSTRACT *(Maximum 200 words)*

A combined microactuator/microsensor system has been developed using silicon micromachining techniques for use in high speed jets and control of screech in these jets. The 14μm-thick electrostatic microactuator was fabricated and tested at the exit of a supersonic axisymmetric jet for the introduction of perturbations into the convectively unstable supersonic shear layer. It can be forced into mechanical resonance at frequencies of 5/14 kHz at an amplitude of >70μm, thus generating significant disturbances into the "macro" scale jet flow, and survive operation at speeds of >210m/s. These microactuators have survived hundreds of experiments in the harsh jet environment, and their performance matches or exceeds that of other "macro" actuators. An array of micromachined sound detectors for the detection of onset of jet screech has also been fabricated. The detectors use stress compensated PECVD silicon nitride/oxide membranes together with monocrystalline ion-implanted p^{++} silicon piezoresistors to achieve high sensitivity. They have a static sensitivity of 1.1μV/V·Pa with a 2% nonlinearity over a pressure range of 10kPa. A chip has been fabricated that supports an array of microactuators and sound detectors. Ongoing investigations are aimed at developing a technique to modify, and ultimately control, the feedback loop responsible for the creation of screech.

14. SUBJECT TERMS

MEMS, microactuators, microsensors

DTIC QUALITY INSPECTED 2

15. NUMBER OF PAGES

16. PRICE CODE

17. SECURITY CLASSIFICATION OF REPORT	18. SECURITY CLASSIFICATION	19. SECURITY CLASSIFICATION OF ABSTRACT	20. LIMITATION OF ABSTRACT
UNCLASSIFIED	UNCLASSIFIED	UNCLASSIFIED	UL

Pressure Sensor Arrays and Microactuators for Fluid Mechanics Research

Final Technical Report

Submitted to

Air Force Office of Scientific Research
Bolling AFB, Washington DC 20332-6448

Grant Number: *F49620-96-0293*
Period Covered: *6/1/96-8/31/97*

Submitted By:

Center for Integrated Sensors and Circuits
Department of Electrical Engineering and Computer Science
University of Michigan
Ann Arbor, Michigan 48109-2122

Technical Contact:
Professor Khalil Najafi, Principal Investigator
2402 EECS Building, 1301 Beal Avenue
Ann Arbor, MI 48109-2122
Tel: (313) 763-6650; FAX: (313) 763-9324
e-mail: najafi@engin.umich.edu

Administrative Contact:
Dr. Neil D. Gerl
Division of Research Development and Administration
Room 1058, Wolverine Tower
3003 S. State Street
Ann Arbor, MI 48109-174
Tel: (313) 763-6438

November 1997

I. Introduction

Development of advanced aircraft requires not only a detailed understanding of the physics of turbulence and fluid dynamics, but also a means to prevent unsteady and potentially dangerous flow conditions. An area of interest in high speed aircraft research is that of the theory of receptivity of the coupling between acoustic waves and shear flow and the resulting screech phenomenon of jets operated under off-design condition [1-3].

Screech is a resonant feedback condition that occurs when shear-layer instability waves interact with the shock system of a supersonic plume. The feedback loop consists of shear-layer disturbances convecting through the shock system. Interaction of the disturbances with the shock cells produces acoustic waves that propagate upstream outside the shear-layer to the nozzle lip. At the nozzle lip shear-layer disturbances are generated by the acoustic waves through receptivity, thus completing the loop (as shown in Figure 1). The feedback loop causes lock-in to a resonant frequency and so screech appears as a high intensity peak in the spectrum at a sharply defined frequency. Jet screech tones generate large acoustic pressure fluctuations which not only produce high noise levels but also could result in structure failure of airplanes due to fatigue.

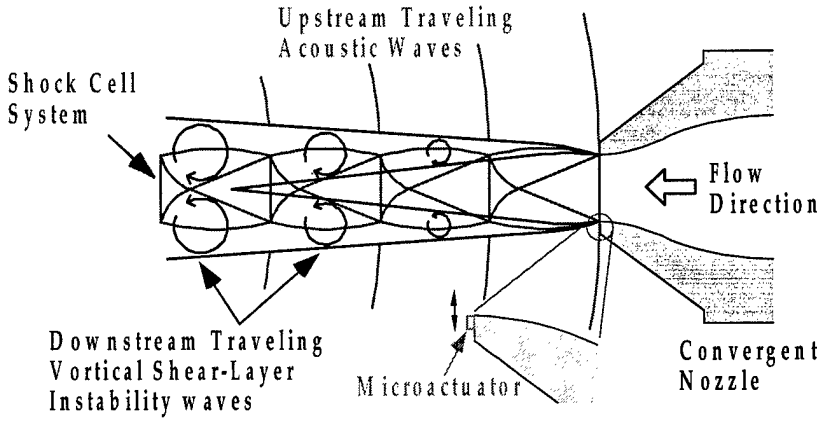

Figure 1: Illustration of screech in high-speed jets.

The primary objective of this research is to investigate the usability of mechanical actuators and sensors, manufactured using MEMS technology, in the control of high-speed, compressible free shear flows. By using an array of microactuators it may be possible to interfere with the screech feedback loop at the point of receptivity where the compressible shear layer disturbances are created by acoustic waves at the nozzle lip. The microactuator array is designed to effectively replace the original nozzle lip with one that can produce different types of disturbance modes, as shown in Figure 1 and Figure 2. Then instability waves will be driven out of phase with the fundamental screech instability mode to cancel the screech tone completely. The screech tone can be detected using an array of sound detectors (pressure sensors), co-integrated with the actuators on the same substrate. This complete sensor/actuator system could be then utilized to develop a closed-loop control system for fluid-mechanics applications.

This basic research effort is conducted in collaboration with colleagues at the Fluid Dynamics Research Center of the Illinois Institute of Technology (FDRC/IIT). The ultimate goal

of this work is to develop a MEMS-based system and utilize it on the High Speed Jet Facility (HSJF) at IIT and conduct research into the active modification and control of screech in supersonic shear layers. This report presents a summary of the results that have been obtained during the past year.

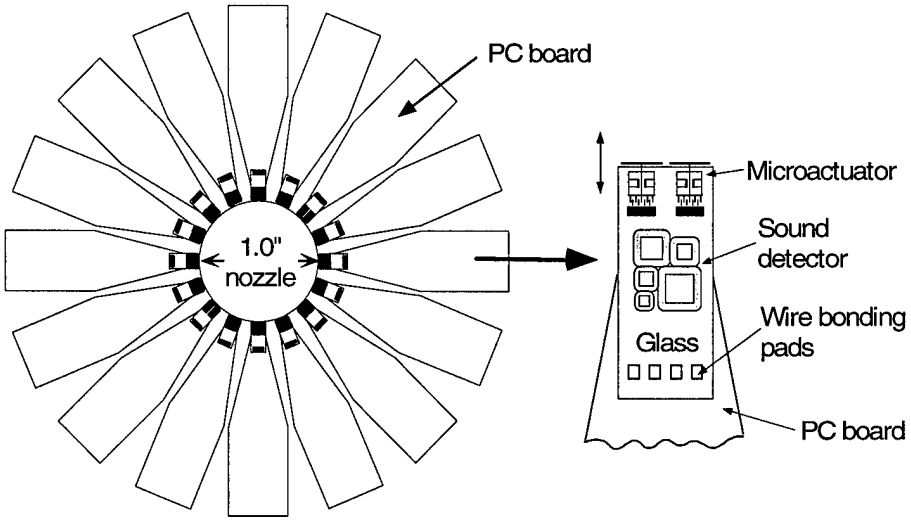

Figure 2: The overall structure of the microactuator/microsensor system. The system consists of a number of microactuators and sound detectors that are all fabricated on a glass substrate and are located around a 1.0" diameter hole.

II. Experimental Approach

Appropriate development of MEMS-based actuators for flow control applications must address two issues: (1) the ability of the micron-size amplitude and forces of the MEMS devices to affect larger-scale flows with orders of magnitude higher energy, and (2) the survivability of the delicate actuators when exposed to the high-speed, highly unsteady flows.

Our approach to the development of a MEMS system utilizes an array of 16 MEMS actuators positioned around the perimeter at the exit of a sonic nozzle, as shown in Fig. 2. To control screech, two strategies based on open and closed loop control methods will be tested. The open loop approach will make use of a few of the actuators (e.g., the top half of the array) to attempt to break the symmetry of the naturally existing flow structures. This is expected to have a similar effect on screech as that produced by intrusive tabs, while having a much smaller effect on the jet thrust due to the extremely small size of the MEMS devices. For this approach, we have used an actuator frequency of 14kHz. An actuator with the higher frequency will provide us a higher survivability under the harsh jet environment.

Alternately, in the closed loop control approach, the MEMS actuators will be used to introduce disturbances that have mode shape and phase such that they counteract the natural shear layer instability modes existing during screech. For this approach, we have chosen an actuator frequency of 5.0 kHz, which corresponds to a region of smooth change in screech frequency [4]. In addition, this value was chosen to take advantage of one of the discontinuous

frequency jumps. Because of the discontinuity, 5.0 kHz actually corresponds to two distinct jet Mach numbers at approximately 1.31 and 1.49. This widens the scope of experimental applications of the actuators by allowing the study of two different jet instability modes.

III. Microactuator/Microsensor Structure

In order to generate sufficient mechanical perturbations into the jet plume at the correct resonant frequency, the actuators should be 1-2mm wide, should not introduce unwanted perturbations (such as thermal) into the jet, should be able to interact with the shear layer of the jet flow by physically intruding into the shear layer, and should be capable of tens of microns of movement at their resonant frequency. This requires that the front portion of the actuator tip overhang the edge of its substrate and enter the shear layer of the jet flow when activated (as shown in Figure 1). Because the screech phenomenon occurs at a velocity for Mach numbers of 1.31 and 1.49, a MEMS device needs to be developed that is capable of functioning in the relatively harsh environment present at the lip of the supersonic jet. Indeed, this is a very challenging task since the jet speeds could approach several hundred meters per second, the flow can contain many particulates that can easily damage the microactuator, and above all, the microactuators are extremely small and delicate devices that have never before been operated under these conditions. These conditions dictate that the actuator must be very compliant in the direction parallel to the substrate, and very stiff perpendicular to the substrate. In order to achieve these requirements, electrostatic actuators that are supported by thick, narrow and long beams can be utilized. Electrostatic actuation is desirable because one can achieve relatively large motions in a small area without generating unwanted thermal disturbances. The great thickness required for large stiffness in one direction can be achieved by using thick micromachined bulk silicon microstructures. In addition, because of their small mass and rather stiff supports, these actuators can be resonated at the high frequency of 5kHz.

Figure 3 shows the overall view of a single comb-drive electrostatic microactuator. The front portion of the microactuator's tip overhangs the edge of its substrate and penetrates the jet flow when activated. In this design, the support anchors for the moving mass are spread out over the entire area of the actuator, thus effectively increasing the stiffness of the actuator in the direction normal to the substrate.

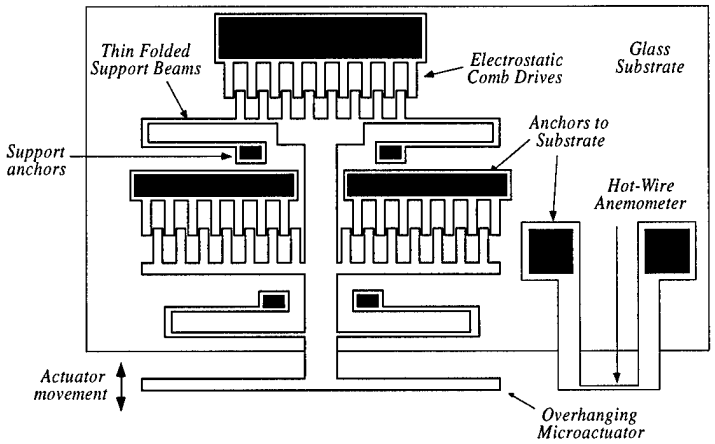

Figure 3: Structure of the electrostatic microactuator.

During last year an additional modification into the design of the actuator was incorporated to make it more robust. In the original design, as shown in Figure 4(a), the tip of the actuator was parallel to the glass edge. This created a problem when the actuator started to move toward the jet nozzle. Only part of the tip (AB) is exposed to the flow while the other part (BC) remains unaffected. The actuator, therefore, becomes unstable because of the imbalance of force acting upon it when there is a high flow. The problem may be solved by rotating the actuators ±11.25° to match the curvature of the one-inch diameter nozzle lip, as shown in Figure 4(b). A SEM view of one of the new actuators can be seen in Figure 5. These actuators can generate an oscillation amplitude of about 88μm peak to peak at the resonant frequency of 5.466kHz using a 60V pulse signal.

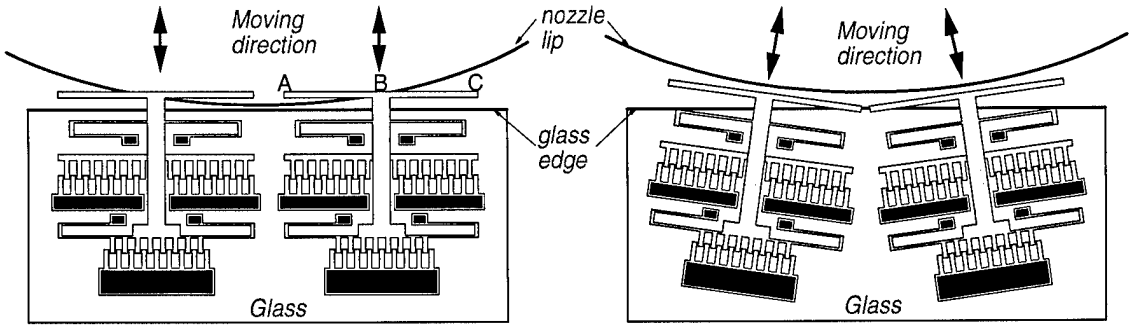

(a) (b)

Figure 4: (a) Second and (b) third generation actuator design.

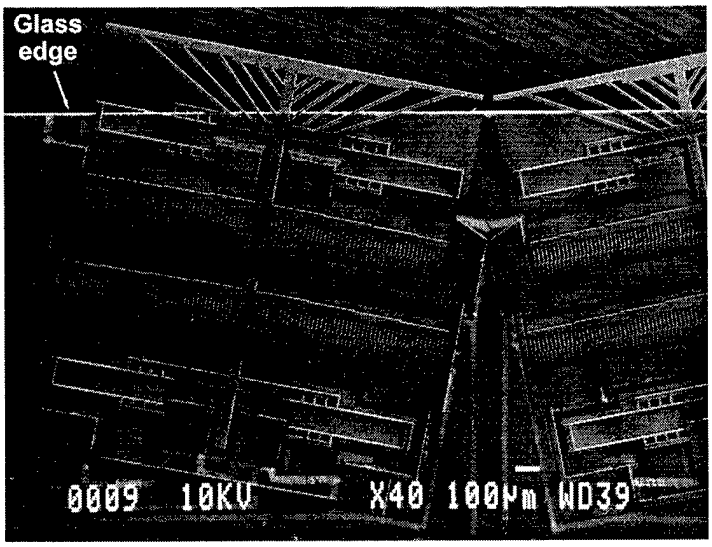

Figure 5: SEM view of two actuators in the new design.

In addition to this new actuator design, we have also designed an array of sound detectors. These detectors have just been fabricated and will be used to measure the phase of the feedback acoustic waves associated with screech. As mentioned before, screech results from instability waves inside the shear layer. In order to effectively control screech, the disturbances

generated from the microactuator should be in the opposite phase of the instability waves. That is, as these two disturbances add together, the resultant will be zero and the screech will be canceled. To this end, an array of sound detectors should be integrated with the microactuators to monitor the phase of the screech. This will allow determination of the appropriate phase of the disturbances generated by the actuators.

Sound detectors or microphones are transducers that convert acoustic energy into electrical energy. Many principles have been developed over the years to achieve this, including the piezoelectric, FET, piezoresistive and capacitive microphones. Although a variety of other techniques are also utilized for building microphones (including electrodynamics and contact carbon microphones), only those that are able to be formed into large arrays using micromachining techniques will be discussed here. The following is a brief explanation of the working principle of each type of microphone.

A. Piezoelectric Microphone

A piezoelectric microphone consists of a thin diaphragm that is either provided with a piezoelectric material or mechanically connected to a bimorph bender, which is a cantilever beam of two layers of piezoelectric material having opposite polarization [5, 6]. A movement of the diaphragm causes stress in the piezoelectric material. The stress generates an electric voltage that can be measured externally. The major disadvantages of this type of microphones are their large device sizes and their difficult fabrication processes. It is hard to combine their process with integrated circuit fabrication, which is desirable when developing large arrays of sound detectors. The sensitivity of many micromachined devices also suffers from the smaller piezoelectric effect of the thin-film materials used. Because of these drawbacks, the piezoelectric microphone will not be used.

B. FET Microphone

Since the signals from the microphone need to be amplified by a pre-amplified circuit, a silicon condenser microphone with an integrated field-effect transistor has been developed [7]. A metallized diaphragm serves as the movable gate of the field-effect transistor. An advantage of the FET microphone is the low output impedance, because the preamplifier is integrated with the microphone. Its disadvantage, however, is its lack of a bias element, which defines a stable gate potential of the FET and prevents the long-term stability of the microphones from being affected by drift. Another disadvantage of the FET microphone is its relatively high noise levels. The FET microphone will therefore not be considered in this work.

C. Capacitive Microphone

A capacitive microphone consists of a diaphragm and a backplate. The change in capacitance in response to the deflection of the diaphragm when exposed to the acoustic pressure waveform provides a measurement of the acoustic pressure. Capacitive microphones can be divided into two main categories: 1) electret microphones, which are biased by a built-in charge, and 2) condenser microphones, which are biased by an external voltage source. Electret microphones will not be discussed here because of their sophisticated processing sequence.

Condenser microphones have received a lot of attention during the past few years because of their relatively high sensitivity [7-10]. There are many different technologies that have been developed for condenser microphones, all aiming at the fabrication of thin diaphragms with large capacitance values for improving signal-to-noise ratio. The electrical sensitivity of the condenser microphone increases with the size of the diaphragm area. However, when the diaphragm area is too large, capacitive devices become less effective in fluid mechanics research because the density of the pressure sensor arrays is relatively decreased. Furthermore, the electrical sensitivity of a capacitive microphone is inversely proportional to the air gap between the diaphragm and backplate. The sensitivity of the microphone will decrease at high frequencies due to the air-streaming resistance of the narrow gap. Therefore, an optimum must be found between sensitivity and frequency response of the microphone.

D. Piezoresistive Microphone

A piezoresistive microphone consists of a diaphragm that is provided with four piezoresistors in a Wheatstone bridge configuration. These resistors are located at the edge of the diaphragm, two of them aligned radially and two aligned tangentially to the diaphragm[1]. If the diaphragm deflects, the strains at the center and the edge of the diaphragm have opposite signs, thus causing an opposite resistance change of the piezoresistors.

An advantage of the piezoresistive microphone is the relatively low output impedance. However, its sensitivity is small compared to a capacitive device, and it also suffers from rather large temperature sensitivity [11]. In spite of these drawbacks, piezoresistive pressure sensors have been extensively used over the years for many different applications, especially those in transportation. Recently, some have started to use this approach to fabricate microphones for fluid mechanics applications [12], but the achievable sensitivity has been small (less than 0.1μV/V/Pa for a 100μm device). Larger devices have also been fabricated with improved performance. From [13], a piezoresistive microphone has been fabricated consisting of a 1 μm thick highly boron-doped silicon diaphragm with an area of 1 mm^2 and four 0.25 μm thick p-type polysilicon resistors, which provides a sensitivity of 4.17 μV/V/Pa with a supply voltage of 6V.

The piezoresistive readout scheme for the sound detector is chosen in this research because of several reasons, including: 1) the sound level of screech is so high (>120dB sound pressure level) that the slightly lower sensitivity of a piezoresistive readout does not limit the performance; 2) the fabrication and readout of a piezoresistive sound detector are much simpler than either a piezoelectric or capacitive microphone; 3) the bandwidth of a piezoresistive device is not affected by air damping typically encountered in a capacitive device with a small air gap; 4) this application does not require a wide and flat frequency response over the entire audio frequency range, as is typically needed in a microphone, since the screech frequency is narrowly located around a few kHz range; and finally 5) since the transduction scheme has to withstand a high level of background noise caused by the high speed flow, a capacitive readout scheme is not preferred because of its higher susceptibility to environmental noise and the need for adequate shielding. A piezoresistive readout scheme can provide sufficient sensitivity, bandwidth, and a simple interface circuit to make it the most suitable for this application. To compensate for the

[1] For p-type resistors in the (100) plane.

lower sensitivity, an ultra thin diaphragm and highly boron-doped piezoresistors have been developed using a fabrication technology compatible with integration with the microactuators.

Because of these features, we have designed a novel, yet simple sound detector. Figure 6 shows the structure of this piezoresistive sound detector and Figure 7 shows the SEM view of a large gap (~20μm) piezoresistive sound detector. The diaphragm consists of three layers of dielectric material with a total thickness of 0.23μm. Four 3μm thick p-type shallow boron diffusion resistors are arranged on the edge of the diaphragm. These resistors have the piezoresistance coefficient, π_{44}, of $43\times10^{-12}(cm^2/dyn)$ [14], which is about four times higher than that of p-type polysilicon piezoresistors. Therefore, this sound detector is expected to be more sensitive than a polysilicon piezoresistive sound detector.

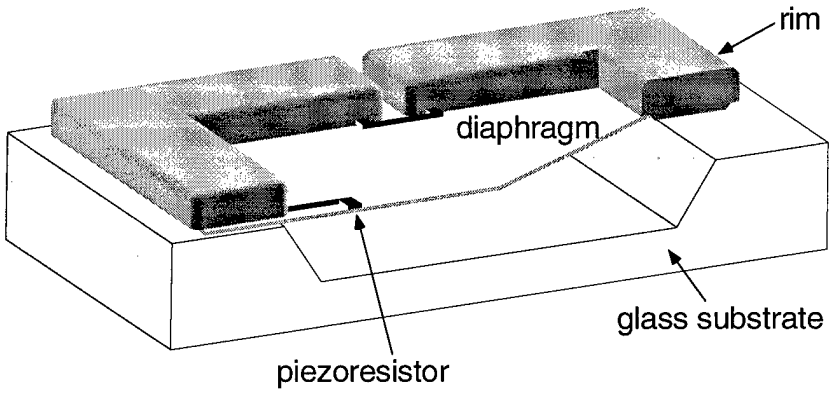

Figure 6: 3D drawing of a Piezoresistive sound detector.

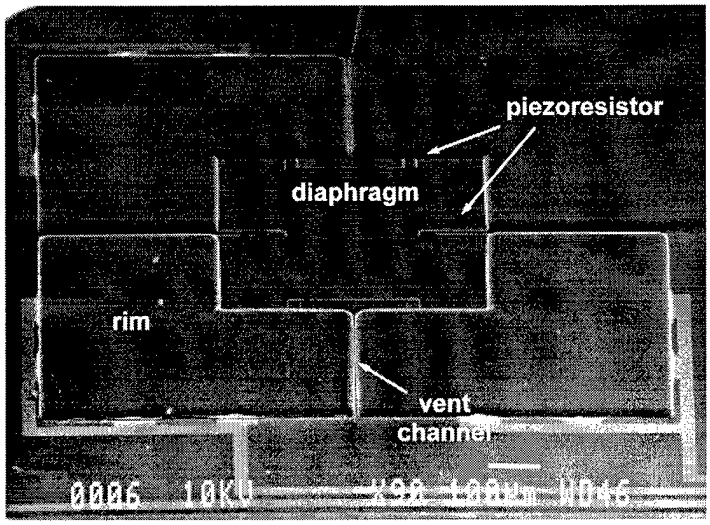

Figure 7: SEM view of a piezoresistive sound detector. The diaphragm is $0.49mm^2$, and 0.23μm thick with four 3μm-thick piezoresistors.

In summary, a piezoresistive sound detector has demonstrated the following:

I. The piezoresistive sound detector is simple and yet effective in measuring the change of sound level.
II. This piezoresistive sound detectors utilize the silicon's high piezoresistive coefficient and low temperature dependence due to its high dopant concentration [14].
III. A very large gap sound detector has been make to reduce the damping effect. This widens the operation range of this sound detector.

IV. Fabrication

Bulk silicon dissolved wafer process has been developed and utilized for the fabrication of many sensors and actuators in the past several years. These devices include pressure sensors [15], accelerometers [16, 17], scanning thermal microscopes [18], and microactuators [19]. The dissolved wafer process has several advantages in the fabrication of the microactuators and microsensors:

1. Simple process: it only takes as few as three masks to construct a microactuator/microsensor system.
2. Versatility: the process enables a designer to change the thickness as well as the shape of a micromachined structure over a large range of values.
3. Rigidity and stability: the thickness of a device depends on the boron diffusion depth (this can be up to 20μm), which allows mechanically rugged and strong devices to be fabricated.
4. Easy packaging: actuators and sensors are anchored to a glass substrate. This increases the strength of the MEMS chips and makes them easier to be handled during packaging.
5. Possibility of creating an overhanging structure: using this process, we are able to create a solid overhanging plate which can penetrate the flow and generate desired disturbances.
6. Compatibility: hot-wire anemometers and pressure sensors can be made by applying the same process.

Figure 8 shows the complete dissolved wafer process which is used to fabricate the microactuator/microsensor system. The device itself is fabricated from micromachined p++ silicon microstructures that are supported on a glass substrate. The head of the actuator and the heater of the hot wire anemometer are located in the proper positions overhanging the edge of the glass substrate and interacting with the jet flow. The fabrication process of the device requires three masks. It starts with an unmasked deep boron diffusion (~15μm) performed at 1175°C for 15 hours, which defines the thickness of the beams and the teeth of the drive combs. The large thickness is critical to this application since it reduces both the drive voltage and the susceptibility to clamping. The boron-diffused areas are then etched anisotropically using reactive ion etching (RIE) in a SF_6/O_2 gas plasma to pattern the fine microstructures needed to form the support beams and the drive combs [18]. This completes the silicon processing. The glass substrate is patterned and recessed to a depth of about 6μm by a mixture of diluted hydrofluoric (HF) and nitric acids to create the bonding anchors. This recess is also critical as it allows the formation of a gap under the silicon structure which needs to be large enough to reduce the clamping of the microactuator to the substrate during both processing and the actual

operation. The formation of such a gap is possible only by using the dissolved wafer process. Glass processing is completed after patterning Ti/Pt/Au interconnect lines on it. Finally, the silicon wafer is electrostatically bonded to the glass wafer, and the sandwich is then immersed in EDP (a concentration-dependent silicon etchant) to dissolve away the undoped silicon, leaving the p++ silicon devices mounted on the glass substrate.

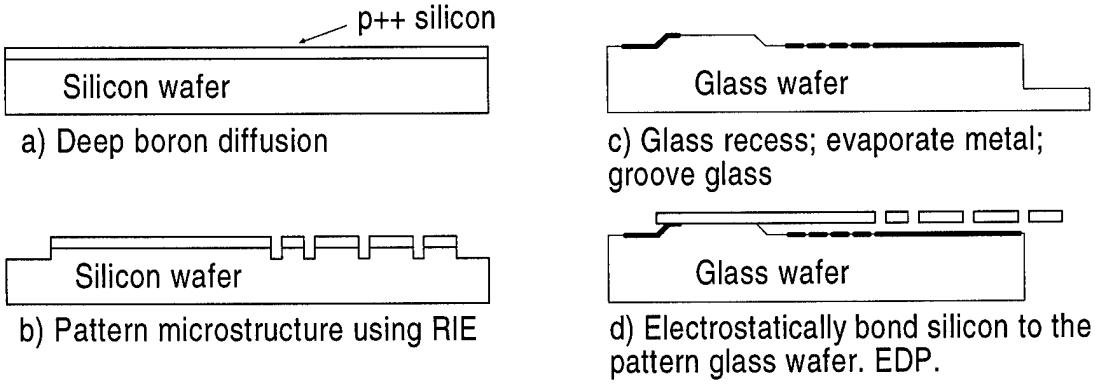

Figure 8: The dissolved wafer process sequence.

In order to make a sound detector, a diaphragm and piezoresistors will be needed. Therefore, some modifications on the original dissolved wafer process are required. Figure 9 shows the modified process. It involves nine masks, starting by recessing the silicon wafer with RIE to 1 micron deep, except in those areas that will later be bonded to the glass substrate to anchor the actuators. This creates equalized channels for sound detectors. Next a selective deep boron diffusion (~15μm) is performed at 1175°C for 15 hours, which defines the thickness of the devices. This step not only defines the area of the microactuators and the rims of the sound detectors but also reduces the loading effect of deep RIE etch later. A selective boron ion implantation is followed to define the piezoresistors. Because a small thickness is desired in these resistors, boron ion implantation is chosen over shallow boron diffusion whose diffusion thickness is about 3μm, about ten times thicker than that from ion implantation. Then an PECVD nitride layer is deposited to form the sound detector diaphragm followed by an LTO layer. The initial stress of the diaphragm can be reduced by using various combination of nitride and oxide [15]. This enhances the sensitivity of the sound detectors due to small initial stress. The wafer is then patterned and metallized with a Ti/Pt layer in areas where lead transfers are to be made to the metal lines on the glass substrate. This improves the sound detector's sensitivity by reducing the contact resistance between the silicon and the metal on the substrate. The boron-diffused areas are then etched anisotropically using reactive ion etching (RIE) in a SF_6/O_2 gas plasma to pattern the fine microstructures for actuators. Because only small areas are needed to be etched, the total etching time is reduced by a half. The wafer is then thinned down to about 100μm using nitric acid and HF. This completes the silicon processing.

The glass processing is similar to the previous process, except that a 20μm deep recess on glass substrate is created to avoid the stiction and to reduce the damping effect on the sound detectors' diaphragm and microstructures.

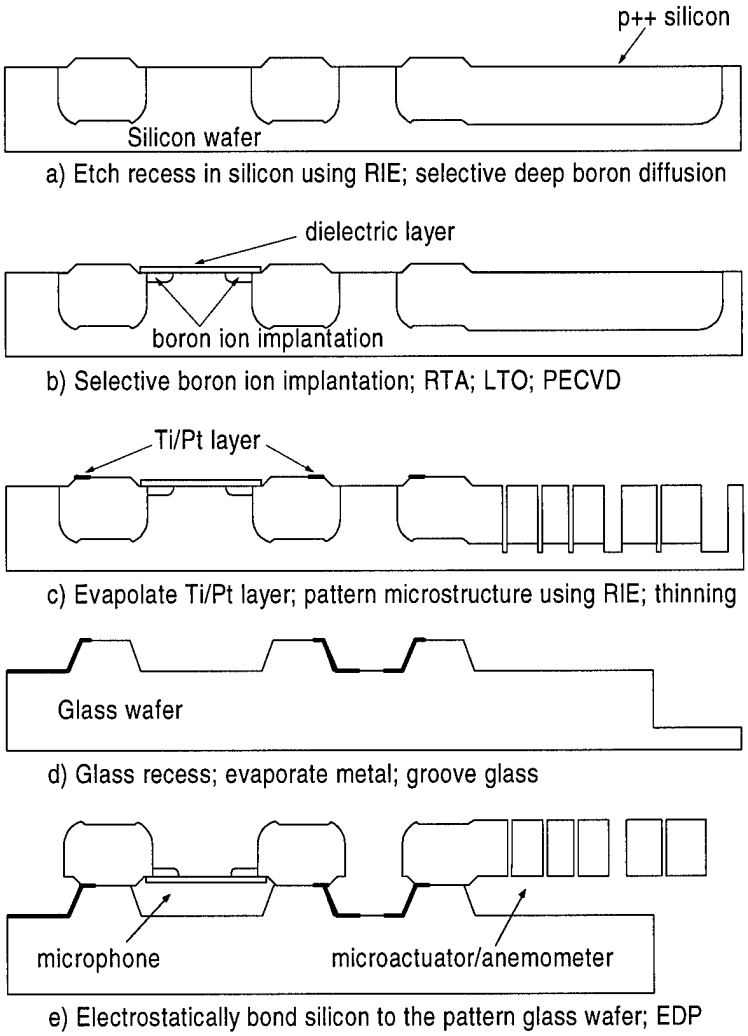

Figure 9: The complete dissolved wafer process sequence for the fabrication of microactuator/microsensor systems.

V. Experimental Results

A. Positioning and Observation of MEMS Operation

As will become evident in the results to be presented later, the effectiveness of the MEMS actuators in exciting the flow is strongly dependent on precise positioning of the devices in the vicinity of the jet lip. Therefore it was necessary to determine with micron accuracy the position of the actuator at the two extreme ends of its motion with respect to the nozzle lip. This was achieved by adjusting the actuator position at the jet exit while viewing it under a microscope at a high magnification of about 50. A high-intensity fiber-optic strobe light was used to illuminate the actuator during observation under the microscope. This resulted in a clearly observable "slow-motion" view of the device while oscillating at frequencies as high as 14 kHz. Measurements of the relative actuator location and its oscillation amplitude were achieved by mounting a CCD camera on the microscope and displaying the video images on a Silicon Graphics Indy work station where measurements were done utilizing the screen pixels after

appropriate calibration. The same optical observation system described above was also used to visualize the operation of the MEMS actuator while running the jet up to speeds corresponding to screech conditions. However, in this case the microscope was positioned at an angle of about 45 degrees with respect to the jet center line, as shown in Figure 10. This oblique angle, combined with the relatively large working distance of the microscope allowed observation of the device during flow conditions without protrusion into the flow. Inspection of a video tape of the actuator operation revealed that the MEMS actuator operated properly with no damage or stoppage due to the large flow speeds and highly unsteady conditions associated with screech.

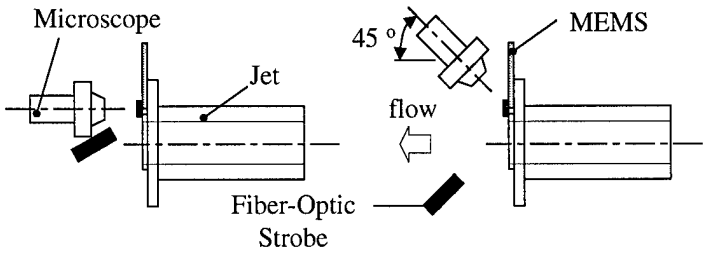

Figure 10: Optical observation system: (a) MEMS mounting, (b) MEMS operation.

B. Detection of the Flow Disturbance Generated by a Single MEMS Device

Prior to implementation of the full MEMS actuator array it was decided to examine the dependence of the strength of the MEMS-produced flow disturbance on various flow and forcing parameters, such as the Mach number, actuator position and amplitude, forcing frequency, etc., for a single MEMS device. This was done in order to allow identification of the appropriate values of these parameters when implementing the full actuator array in the screech control problem.

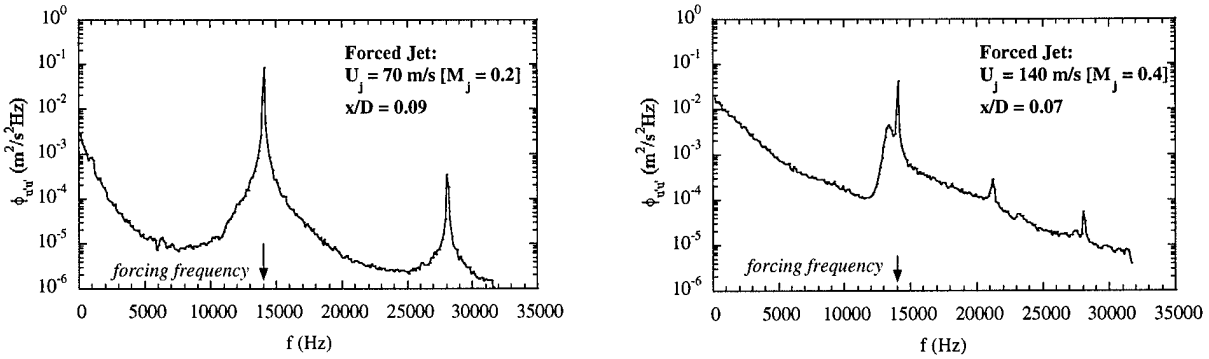

Figure 11: Streamwise velocity spectra when forcing the jet using the 14 kHz actuator.

To test if the MEMS actuator is able to generate a flow disturbance, the spectrum of the streamwise fluctuating velocity (u') was measured at different streamwise (x) locations on the center line of the jet shear layer (where $U/U_j = 0.5$: U is the local mean velocity and U_j is the jet velocity) for different Mach numbers. The measurements were repeated for two different

actuators with resonant frequencies of 5 kHz and 14 kHz. Figure 11 provides a sample of the measured spectra for a single streamwise location and two different Mach numbers for the high-frequency actuators. A very strong peak is observed at the forcing frequency for a Mach number of 0.2 (Figure 11a). In addition to the peak at the forcing frequency, a second strong peak at 28 kHz is also observed. For a Mach number of 0.4, a clear peak is depicted in the spectrum at the forcing frequency, as seen from Figure 2b. The peak magnitude is about an order of magnitude larger than a broad spectrum peak which seems to exist at about 13 kHz, slightly to the left of the forced peak.

C. Magnitude of the MEMS-Induced Disturbances

To evaluate the level of the disturbance introduced into the shear layer by the MEMS actuator, the *rms* content of the spectral peak at the forcing frequency ($<u_{rms,f}>$) was calculated. The forced disturbance *rms* dependence on the streamwise location for Mach numbers of 0.2, 0.4 and 0.6 is shown in Figure 12. The disturbance *rms* is normalized by the jet velocity and the streamwise coordinate is normalized by the jet diameter. Inspection of Figure 12 shows that for both M_j = 0.2 and 0.4 no region of linear growth is detectable. For these two Mach numbers, $<u_{rms,f}>$ only increases slightly before reaching a peak followed by a gradual decrease in value: a process which is reminiscent of non-linear amplitude saturation.

To "gauge" the magnitude of the MEMS forcing it is compared to other types of "macro-scale" forcing. To this end, the disturbance *rms* value produced by internal acoustic (Lepicovsky et al [20]) and glow discharge (Corke and Cavalieri [21]) forcing is compared to the corresponding rms values produced by MEMS forcing in Figure 13. The results for MEMS forcing contained in the figure are those obtained using the high- (14 kHz) and low-frequency (5kHz) MEMS actuators.

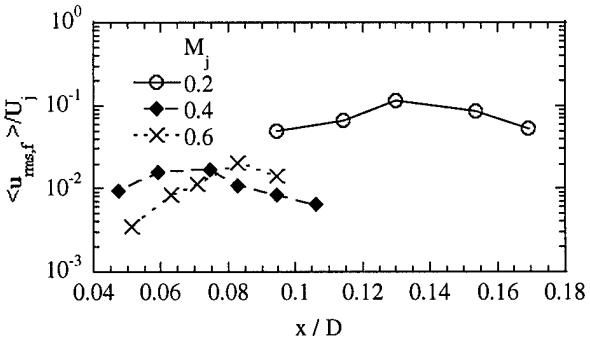

Figure 12: Streamwise dependence of the MEMS-induced disturbance energy for the 14 kHz actuator.

As seen from Figure 13, for all cases of MEMS forcing, except that for the low frequency actuator/M_j = 0.42, the MEMS-generated disturbance grows to a level which is similar to or larger than that produced by glow discharge and acoustic forcing. Furthermore, the power required to drive the MEMS actuator was measured to be 1 mW. This demonstrates one of the main advantages of MEMS-based systems in flow applications similar to the current one: the ability to provide efficient control with large effect-to-expenditure ratios. For M_j = 0.42, the 5 kHz MEMS actuator produces a small disturbance level. However, as will be demonstrated next,

the level of the MEMS-generated disturbance is highly dependent on accurate positioning of the actuator at or very close to an optimal forcing location. For the results for $M_j = 0.42$, no special provisions were taken to ensure that the device was positioned as close as possible to its optimal position. This could affect the outcome by an order of magnitude.

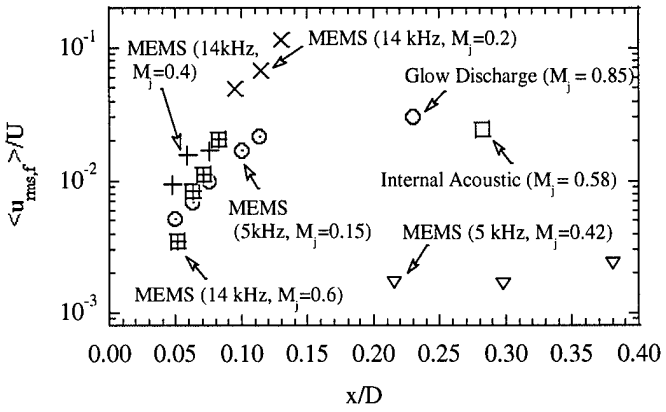

Figure 13: MEMS-induced disturbance level compared to other types of "macro-scale" forcing.

D. Jet Receptivity

The results in Figure 14 suggest that the ability of the MEMS-based actuators in initiating disturbances in the shear layer does not diminish with increasing Mach number. On the contrary, an increase of flow receptivity to MEMS-based actuators is observed at the Mach number increases, demonstrating the ability of MEMS devices to excite high-speed compressible jet flows. The ability is believed to stem from the fact that the MEMS-based actuators are able to provide a focused disturbance to the high-receptivity point at the exit of the jet where the shear layer separates. This high sensitivity to minute disturbances allows devices with small forcing amplitude and energies to affect the flow.

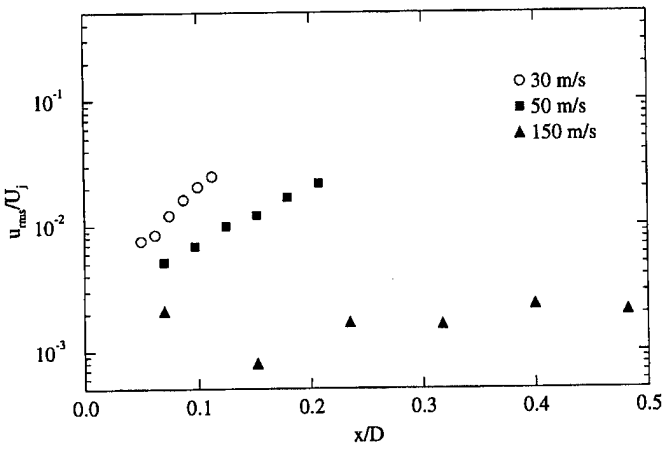

Figure 14: Jet receptivity to excitation by the MEMS devices.

E. Significance of the Jet Lip

The ability of the MEMS devices to excite flow disturbances at a level comparable to that produced by other large-scale forcing, notwithstanding the MEMS micron-size amplitude and force, is believed to be due to the ability to position the MEMS extremely close to the point of high-receptivity at the nozzle lip where the flow is sensitive to minute disturbances. To investigate this matter further, the radial position of the MEMS actuator with respect to the nozzle lip (y_{off}) was varied systematically. The *rms* of the spectral peak at the forcing frequency was calculated for all actuators positions. The results are displayed in Figure 15 for a jet velocity of 70 m/s as a function of the actuator radial position. For reference, a dimension indicating the momentum thickness of the boundary layer, θ_0, emerging at the exit of the jet is included in Figure 15. The initial momentum thickness was estimated by measuring the shear layer momentum thickness at various streamwise (x) location close to the nozzle lip and extrapolating the results to x=0. For the case of M_j = 0.2, the initial momentum thickness is 72μm [22]. As seen from the figure, the largest disturbance energy is produced when the actuator is into flows about 20μm (y_{off} = -20μm). If the actuator is placed a distance as small as 75 μm off the position corresponding to the maximum shear layer response, an order of magnitude reduction in disturbance *rms* value is observed. Figure 15 highlights the significance of the ability to force the shear layer in the immediate vicinity of the jet lip, as discussed earlier. It should be noted that the change of the jet Reynolds and Mach number will affect the result in Figure 15.

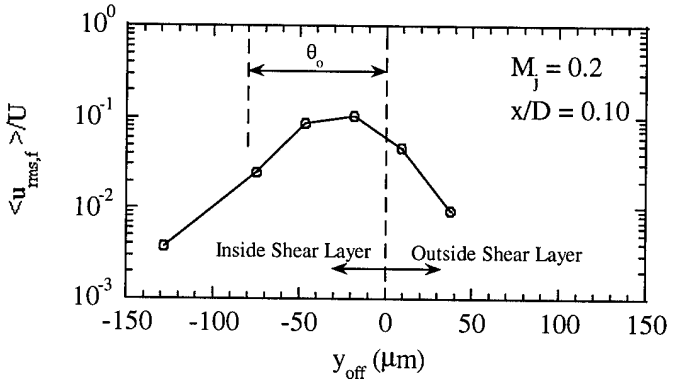

Figure 15: Effect of MEMS actuator radial position on the generated shear layer disturbance level.

F. Testing Results Of Sound Detectors

As mentioned earlier, a 20mm-gap piezoresistive sound detector has been fabricated, which utilizes the silicon's high piezoresistive coefficient and low temperature dependence. An electrical model has been developed for the sound detector, as shown in Figure 16 [23]. R_r and L_r represent the acoustic radiation resistance and mass, L_d and C_d the effective mass and the compliance of the diaphragm, L_{eq} and R_{eq} the acoustic impedance of the equalization channels, R_{gap} the air-streaming resistance of the air-gap, and C_{bc} the compliance of the backchamber, respectively. Based on this model, a static sensitivity of 1.2μV/V·Pa and an acoustic sensitivity of 0.42μV/V·Pa are calculated.

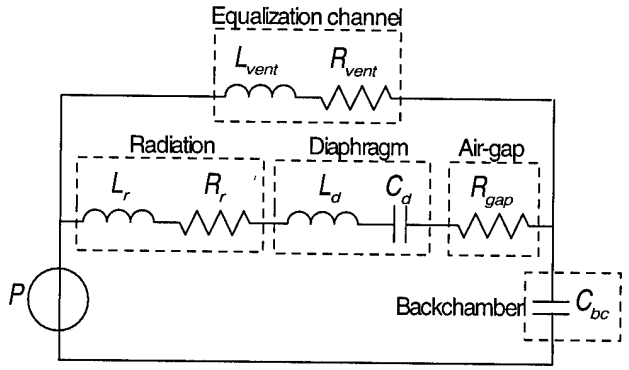

Figure 16: Equivalent circuit for the sound detector.

In spite of the advantages of this sound detector, some improvements are needed for better performance. Figure 17 shows the measured output voltage at various applied pressures after the sound detector is sealed and treated as a pressure sensor. The measured output voltage is amplified by a instrumentation amplifier of gain of 41.6. The bridge bias is 10V. As can be seen, the result is not linear as we expected and the sensitivity is also lower. The sensitivity is about 1.5×10^{-10}V/V·Pa when the pressure is close to ambient but the sensitivity is about 3.69×10^{-8}V/V·Pa when the pressure is close to -100kPa. In fact, there are two problems in this piezoresistive sound detector. First, because of their large thickness, the resistors prevent the diaphragm from deflecting. To overcome this problem, boron ion implantation can be used to define the piezoresistors and can give thinner resistors as mentioned before. Second, the high contact resistance between metal and silicon leads to a low sensitivity. In order to reduce its contact resistance, the silicon wafer is patterned with a metal layer in areas where lead transfers are to be made to the metal lines on the glass substrate [24].

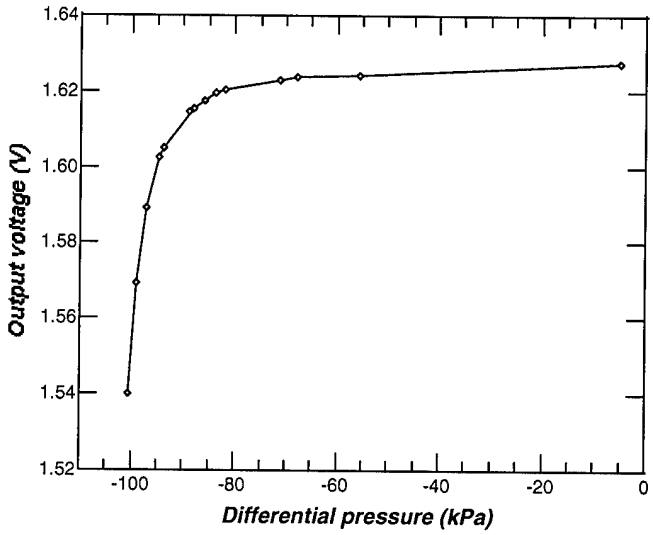

Figure 17: Pressure response of the sound detector. The negative sign on the pressure scale denotes that the pressure in the chamber is lower than that in the cavity of the microphone.

Figure 18 shows an SEM view of one of the modified sound detectors, fabricated with the actuators (shown in Figure 19). These modified detectors consist of a 0.4μm-thick

diaphragm and four 0.2 μm-thick p^{++} ion-implanted piezoresistors with high piezoresistive coefficient. Figure 20 shows the measured pressure sensitivity of the sound detector, which is 1.1μV/V·Pa with a nonlinearity of 2% over the full scale pressure range of 10kPa. The disagreement with the theoretical value for the static sensitivity is due to the uncertainty of the intrinsic stress and the Young's modulus of the dielectric diaphragm.

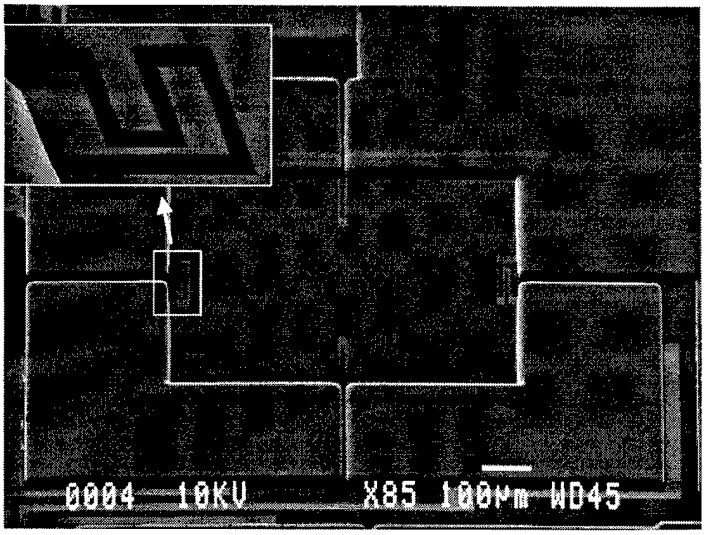

Figure 18: SEM view of a 710μm-square silicon sound detector and a close-up view (on the upper left corner) of one of the piezoresistors.

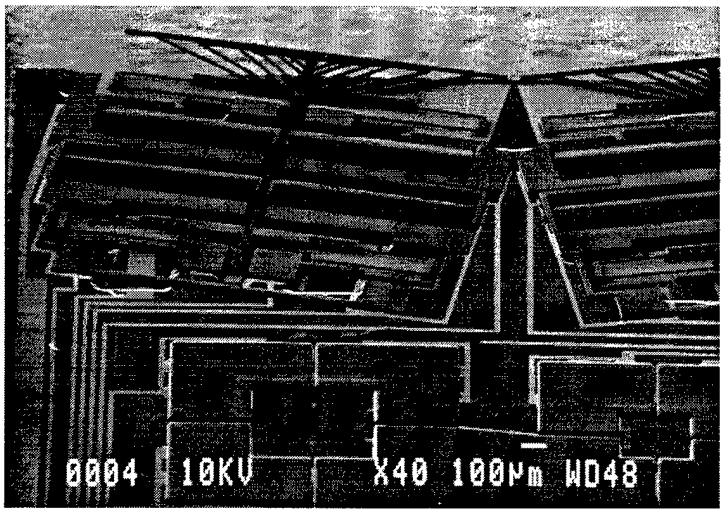

Figure 19: SEM view of sound detectors and two microactuators.

Figure 21 shows the measured pressure sensitivity of a sound detector at two temperatures. The temperature coefficient of sensitivity is 4145*ppm*/°C. An overload pressure of 50kPa has been applied onto these devices without damage to their diaphragm. This demonstrates the robustness of the sensors for use in detecting jet noise. Under the screech condition, the sound pressure level of screech is about 120dB, which is equivalent to a sound

pressure of 20Pa. According to simulation, the output voltage will be 82μV under a bias voltage of 10V. Further testing in jet noise is yet to be performed on these detectors.

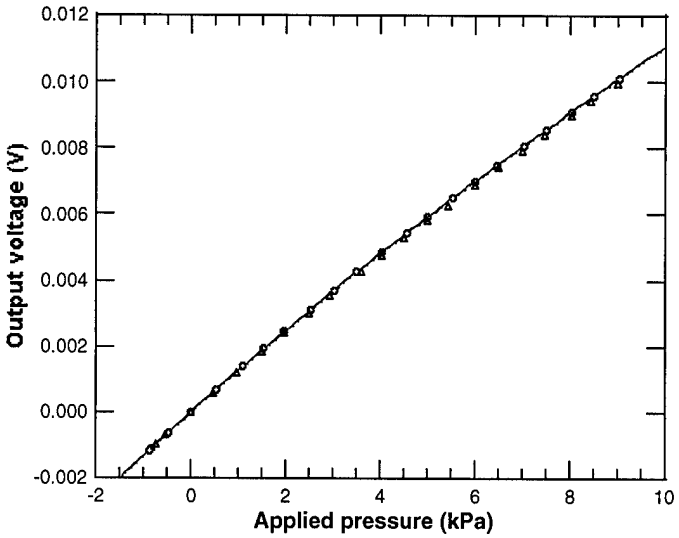

Figure 20: Measured pressure sensitivity for the sound detector.

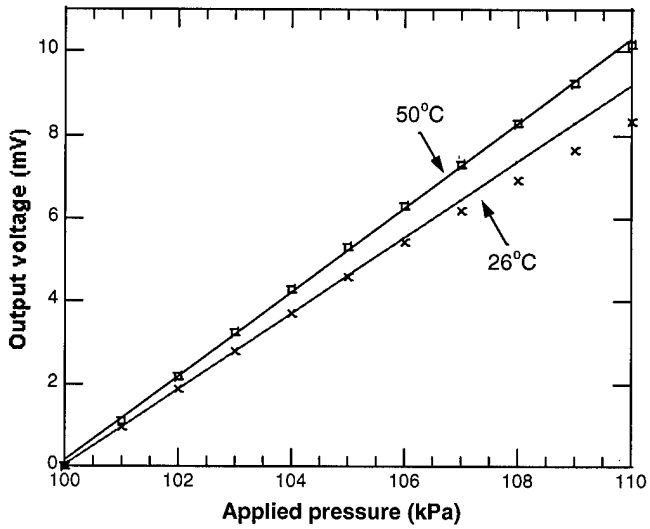

Figure 21: A pressure sensitivity of 0.92μV/V·Pa is measured with a temperature coefficient of sensitivity (TCS) of 4145*ppm*/°C.

VI. Conclusions

During the past year, we have provided our colleagues at IIT a large number of actuators for testing in their high-speed jet facility. As mentioned before, one of the main goals of this research was to design and fabricate miniature actuators and sensors, and to investigate their usability to affect large-scale flows. The project has been successful in terms of this objective. Two types of actuators have been fabricated using the dissolved wafer process. One has a

resonant frequency of 5kHz with an actuation amplitude of at least 60μm peak to peak. The other has a resonant frequency of 14kHz with similar actuation amplitude.

The effectiveness of MEMS-based mechanical actuators in exciting incompressible as well as compressible jet flows has been demonstrated for flow speeds up to 240m/s for the 5kHz and 14kHz actuators. The level of the introduced disturbances into the shear layer is similar to or larger than that produced by the other conventional types of forcing. It has also been demonstrated that the disturbance level is strongly dependent on the proximity of the actuator to the jet lip, or the high receptivity point in the flow. The success of the MEMS device with its small size in exciting the jet flow has been attributed to the ability to position the actuators extremely close to the lip where the flow is extremely sensitive to minute disturbances.

An additional improvement for the microactuator/microsensor design was incorporated to meet the need of this project. First, the overhanging parts of the actuators have been designed to match the curvature of the nozzle lip by rotating the actuators ±11.25°. This modification has solved the problem of the imbalance force acting upon the overhanging tip of the actuator when the actuator started to move toward the jet nozzle. These actuators can generate an amplitude of about 88μm peak to peak at the resonant frequency of 5.466kHz using a 60V pulse signal. Second, an array of sound detector has been designed to monitor the phase of the feedback acoustic waves associated with screech. Furthermore, in order to integrate the sound detector with actuator together, a new fabrication process has been design. Further testing of the actuators and the sound detectors on HSJF at IIT will be conducted in the future.

VII. References

[1] D. W. Bechert, and B. Stahl, "Shear Layer Excitation, Equipment vs. Theory," DFVLR TR No. DFVLR-FB pp. 84-26, 1984.

[2] D. G. Crighton, "The Kutta Condition in Unsteady Flow," Ann. Rev. *Fluid Mech.*, 17, pp. 411-445, 1985.

[3] R. E. Drubka, P. Reisenthel, and H. M. Nagib, "The Dynamics of Low Initial Disturbance Turbulent Jets," *Phys. Fluids* A, 1, pp. 1723-1735, 1989.

[4] Joseph Papp, "Application of Micro-Electro-Mechanical Actuators in the Investigation of Supersonic Jet Screech," Master thesis, Illinois Institute of Technology, 1996.

[5] R. Schellin, G. Hess, W. Kuehnel, G. M. Sessler, and E. Fukada,, "Silicon Subminiature Microphones with Organic Piezoelectric Layers," *IEEE Trans. on Electrical Insulation,* Vol. 27 No. 4, August 1992.

[6] Eun Sok Kim, and Richard S. Muller, "IC-Processed Piezoelectric Microphone," *IEEE Electron Device Letters,* Vol. EDL-8, NO.10, October 1987.

[7] W. Kühnel and G Hess, "Micromachined Subminiature Condenser Microphones in Silicon," *Sensors and Actuators A*, Vol. 32, pp. 560-564, 1992.

[8] J. Bergqvist and F. Rudolf, "A New Condenser Microphone in Silicon," *Sensors and Actuators A*, Vol. 21-23, pp. 123-125, 1990.

[9] J. Bergqvist, F. Rudolf, J. Maisano, F. Parodi and M. Rossi, "A Silicon Condenser Microphone with a Highly Perforated Backplate," *Proc. 6th Int. Conf. Solid-State Sensors and Actuators Transducers '91*, pp. 266-269, June 1991.

[10] T. Bourouina, S. Spirkovitch, F. Baillieu and C. Vauge, "A New Silicon Condenser Microphone with a P+ Silicon Membrane," *Sensors and Actuators A*, Vol. 31, pp. 149-152, 1992.

[11] Steve T. Cho, "An Ultrasensitive Silicon Pressure-Based Microflow Sensor," Ph.D. Dissertation, the University of Michigan, 1991.

[12] Edvard Kälvesten, "Pressure and Wall Shear Stress Sensors for Turbulence Measurements," Ph.D. Dissertation, Royal Institute of Technology, 1996.

[13] R. Schellin and G. Hess, "A Silicon Subminiature microphone Based on Piezoresistive Polysilicon Strain Gauges," *Sensors and Actuators A,* Vol. 32, pp. 555-559, 1992.

[14] Yozo Kanda, "Piezoresistance effect of silicon," *Sensors and Actuators A,* Vol. 28, pp. 83-91, 1991.

[15] Yafan Zhang, "Non-Planar Diaphragm Structures for High Performance Silicon Pressure Sensors," Ph.D. Dissertation, the University of Michigan, 1994.

[16] Karl J. Ma, "An Active Dissolved Wafer Process for the Fabrication of Integrated Sensors," Ph.D. Dissertation, the University of Michigan, 1994.

[17] Chingwen Yeh, "A Low-Voltage Bulk-Silicon Tunneling-Based Microaccelerometer with CMOS Interface Circuitry," Ph.D. Dissertation, the University of Michigan, 1996.

[18] Y. Gianchandani, and K. Najafi, "A Silicon Micromachined Scanning Thermal Profiler with Integrated Elements for Sensing and Actuation," In Press, *IEEE Trans. Electron Devices*, 1997.

[19] C. Huang, J. Papp, K. Najafi, H. Nagib, "A Microactuator System for the Study and Control of Screech in High Speed Jets," *Proc. Ninth Annual Int. Workshop on MEMS,* pp. 19-24, Feb. 1996.

[20] J. Lepicovsky, K. K. Ahuja, and R. H. Burrin, "Tone Excited Jets, Part III: Flow Measurements," *Journal of Sound and Vibration* 102 (1), pp. 71-91. 1985.

[21] T. C. Corke and D. Cavalieri "Mode Excitation in a Jet at Mach 0.85". 49th American Physical Society Meeting, DFD, Syracuse, NY. 1996.

[22] A. Naguib, C. Christophorou, E. Alnajjar, H. Nagib, C. Huang, and K. Najafi, "Arrays of MEMS-Based Actuators for Control of Supersonic Jet Screech," *American Institute of Aeronautics and Astronautics,* Paper 97-1963. 1997.

[23] Mario Rossi, "Acoustics and Electroacoustics" Artech House, Norwood, 1988.

[24] Janet Kay Robertson, "An Electrostatically-Actuated Integrated Microflow Controller," Ph.D. Dissertation, the University of Michigan, 1996.

VIII. Personnel Supported

1. Professor Khalil Najafi: Principal Investigator. Supported at a level of 10% through cost sharing provided by the University of Michigan.

2. C. Huang, Graduate Student Research Assistant, 50% Appointment: Microactuator design, simulation, and fabrication.

IX. Publications

1. C. Huang, K. Najafi, E. Alnajjar, C. Christophorou, A. Naguib, and H. Nagib, "Operation and Testing of Electrostatic Microactuators and Micromachined Sound Detectors for Active Control of High Speed Flows," to be presented at the *IEEE/ASME Micro Electro Mechanical Systems Workshop*, Germany.

2. E. Alnajjar, A. Naguib, H. Nagib, and C. Christophorou, "Receptivity of High-Speed Jets to Excitation Using An Array of MEMS-Based Mechanical Actuators," Proceedings, 1997 *ASME Fluids Engineering Division Summer Meeting*. Paper FEDSM97-3224, 1997.

3. A. Naguib, C. Christophorou, E. Alnajjar, H. Nagib, C. Huang, and K. Najafi, "Arrays of MEMS-Based Actuators for Control of Supersonic Jet Screech," *American Institute of Aeronautics and Astronautics,* Paper 97-1963, 1997.

X. Interactions/Transitions

None

XI. New Discoveries, Inventions, or Patent Disclosures

None